MIT Libraries | DSpace@MIT

MIT Open Access Articles

Epithelial Relaxation Mediated by the Myosin Phosphatase Regulator Mypt1 Is Required for Brain Ventricle Lumen Expansion and Hindbrain Morphogenesis

The MIT Faculty has made this article openly available. ***Please share*** how this access benefits you. Your story matters.

Citation: Gutzman, J. H., and H. Sive. "Epithelial relaxation mediated by the myosin phosphatase regulator Mypt1 is required for brain ventricle lumen expansion and hindbrain morphogenesis." Development 137 (2010): 795-804.

As Published: http://dx.doi.org/10.1242/dev.042705

Publisher: Company of Biologists Ltd.

Persistent URL: http://hdl.handle.net/1721.1/66551

Version: Author's final manuscript: final author's manuscript post peer review, without publisher's formatting or copy editing

Terms of use: Creative Commons Attribution-Noncommercial-Share Alike 3.0

Massachusetts Institute of Technology

Epithelial relaxation, mediated by the myosin phosphatase regulator *mypt1*, is required for brain ventricle lumen expansion, and hindbrain morphogenesis.

Jennifer H. Gutzman[1] and Hazel Sive[1,2†]

[1]Whitehead Institute for Biochemical Research

Nine Cambridge Center, Cambridge, MA 02142

and [2]Massachusetts Institute of Technology

77 Massachusetts Ave., Cambridge, MA 02139

† corresponding author

tel: 617-258-8242; fax: 617-258-5578; email: sive@wi.mit.edu

Running Title: MYPT1 and hindbrain morphogenesis

Keywords: myosin, mypt1, neuroepithelium, rhombomere, brain ventricle, lumen, epithelial relaxation, morphogenesis, hindbrain, cell shape.

SUMMARY

We demonstrate that, in the zebrafish hindbrain, cell shape, rhombomere morphogenesis, and unexpectedly, brain ventricle lumen expansion, depend on the contractile state of the neuroepithelium. The hindbrain neural tube opens in a specific sequence, with initial separation along the midline at rhombomere boundaries, subsequent openings within rhombomeres, and eventual coalescence of openings into the hindbrain ventricle lumen. A mutation in the myosin phosphatase regulator, *mypt1*, results in a small ventricle, due to impaired stretching of the surrounding neuroepithelium. Although initial hindbrain opening remains normal, *mypt1* mutant rhombomeres do not undergo normal morphological progression. 3D reconstruction demonstrates cell shapes within rhombomeres and at rhombomere boundaries are abnormal in *mypt1* mutants. Wild type cell shape requires that surrounding cells be wild type, while mutant cell shape is autonomously regulated. Supporting the requirement for regulation of myosin function during hindbrain morphogenesis, wild type embryos show dynamic levels of phosphorylated myosin regulatory light chain (pMRLC). In contrast, mutants show continuously high pMRLC levels, with concentration of pMRLC and myosin II at the apical side of the epithelium, and myosin II and actin concentration at rhombomere boundaries. Brain ventricle lumen expansion, rhombomere morphology, and cell shape are rescued by inhibition of myosin II function, indicating that each defect is a consequence of overactive myosin. We suggest the epithelium must "relax", via activity of myosin phosphatase, in order to allow for normal hindbrain morphogenesis and expansion of the brain ventricular lumen. Epithelial relaxation may be a widespread strategy to facilitate tube inflation in many organs.

INTRODUCTION

During vertebrate brain development, the lumen of the neural tube fills with embryonic cerebrospinal fluid (eCSF) to form the brain ventricles, a conserved system of interconnected cavities, essential for neurogenesis and normal brain function (Gato and Desmond, 2009; Lowery and Sive, 2009). Brain ventricle formation is intimately connected to morphogenesis of the neuroepithelium. In the hindbrain, rhombomeres are segments of neurectoderm that differentiate into specific cranial nerves. Rhombomeres are morphologically apparent during neural tube and initial brain ventricle formation, but concomitant with ventricle lumen expansion, rhombomeres lose morphological distinctness, although they retain different molecular identities (Hanneman et al., 1988; Heyman et al., 1993; Moens and Prince, 2002).

Zebrafish mutants lacking eCSF fail to form a brain ventricular lumen, confirming the role of fluid secretion in inflating the ventricular lumen (Lowery and Sive, 2005). However, several zebrafish mutants with abnormal ventricle shape do not appear to have defects in eCSF secretion (Lowery et al., 2008). One such mutant corresponds to Mypt1, a regulatory inhibitor of myosin phosphatase. Myosin phosphatase regulates the phosphorylation state of myosin regulatory light chain (MRLC) which, in turn regulates contractility of non-muscle myosin II. In order for myosin phosphatase to be functional, Mypt1 must be non-phosphorylated, and bound to PP1 (the catalytic subunit of myosin phosphatase). Thus, phosphorylated Mypt1 inhibits myosin phosphatase activity (Hartshorne et al., 2004), and mutations in Mypt1 that prevent binding to PP1, result in non-functional myosin phosphatase (Huang et al., 2008).

Cell shape and movement are intimately correlated with myosin function (Lecuit and Lenne, 2007; Quintin et al., 2008). In *Drosophila*, myosin II is required for morphogenetic furrow formation during eye development and for regulation of cell shape and arrangement within the eye imaginal disc (Escudero et al., 2007). Myosin II is required for proper sheet movement and cell shape during Drosophila dorsal closure (Mizuno et al., 2002; Tan et al., 2003). In zebrafish, Mypt1 is important for kidney formation and for convergent extension during gastrulation (Huang et al., 2008; Weiser et al., 2009).

The role of myosin during vertebrate hindbrain formation is not understood. We demonstrate that regulation of myosin function through Mypt1, is required for normal hindbrain cell shape, rhombomere morphogenesis, and, unexpectedly, for brain ventricle lumen expansion, through a process we have termed "epithelial relaxation". This process may play a role during tube lumen expansion in multiple organs.

MATERIALS AND METHODS

Fish lines and husbandry

Zebrafish were maintained and staged using standard procedures (Kimmel et al., 1995; Westerfield, 1995). Zebrafish lines included wild-type AB and *mypt1*^{hi2653} kindly provided by Nancy Hopkins (Amsterdam et al., 2004). Mutant identification information and primers are available upon request.

Brightfield brain imaging, ventricle injections, and forced neuroepithelial expansion

Brain ventricle injections were carried out as described (Gutzman and Sive, 2009). Forced expansion was conducted as above with increased injection pressure (30 psi) for extended time and captured with video. The ventricle opening was measured at the ear before injection and at the point of maximal expansion during injection.

Antisense morpholino oligonucleotide injections

A splice site blocking morpholino-modified oligonucleotide ("morpholino":MO) 5'-ATT TTT TGT GAC TTA CTC AGC GAT G 3' (Gene Tools, LLC) which targets exon 2-intron 2 of zebrafish *mypt1* was injected into one-cell stage embryos. Gene Tools standard 5'-CCT CTT ACC TCA GTT ACA ATT TAT A -3' was used as the control MO.

Live confocal imaging

Live embryo imaging was conducted as described (Gutzman et al., 2008). Embryos were imaged by spinning disk laser microscopy (Perkin Elmer Ultraview RS) for time-lapse experiments. Images were analyzed using Imaris (Bitplane) or Photoshop (Adobe).

Western blot analysis

Wild type embryos were injected with 5 ng of either *mypt1* splice site MO or control MO. The head/brain portion of each embryo was removed posterior to the ear and anterior to the first somite and collected in buffer containing 25mM Tris pH 8.0, 2mM EDTA pH 8.0, 10% glycerol, 1% Triton X-100 plus protease inhibitor. Phospho-MRLC (Cell

Signaling, #3671, 1:1000), β-actin (Sigma, A5441, 1:1000). Films were scanned and quantified using Photoshop (Adobe).

Immunohistochemistry

Embryos were fixed in Dents (myosin II) or in 4% paraformaldehyde (phosphorylated MRLC), blocked in 5% NGS in PBT, incubated in primary antibody (Anti-myosin IIA, M 8064, Sigma, 1:500; phospho-MRLC #3671, Cell Signaling, 1:20) and incubated in secondary antibody (goat anti-rabbit or anti-mouse IgG Alexa Flour 488, Invitrogen, 1:500), some in combination with propidium idodide (PI) (Invitrogen P3566, 1:1000). Actin staining was conducted as previously described (Gutzman et al., 2008). Images were analyzed using Imaris (Bitplane), LSM software (Zeiss), and Photoshop (Adobe). For vibratome sections, fixed embryos were embedded in 5% low-melt agarose. 50 μm sections were stained as described above.

Mosaic analysis

Wild type embryos were co-injected with 5ng control MO or 5ng *mypt1* MO and either memCherry (kindly provided by Dr. Roger Tsien, University of California San Diego) or memGFP mRNA at the one-cell stage. Cells were transplanted from the memGFP injected donors at sphere stage to memCherry injected hosts at shield stage targeted to the presumptive hindbrain (Woo and Fraser, 1995). Transplanted embryos were imaged at 19 hpf by scanning confocal microscopy.

3D cell reconstruction

Confocal images were imported into 3D Doctor (Able Software Corp.). Single cells in r4 and at the r4/r5 boundary were chosen to reconstruct in 3D based on the ability to see an entire cell from the apical to basal side of the neuroepithelium through a z series. Individual cells were manually outlined in each z-section and rendered in 3D. For mosaic analysis, transplanted cells were reconstructed using automated surface rendering of the green channel (transplanted cells) in Imaris (Bitplane).

Blebbistatin treatment

Wild type and *mypt1* mutant embryos were treated with either 50 μm blebbistatin (B0560 Sigma) or 0.1% DMSO control at 22 hpf. After treatment embryos were imaged by brain ventricle injection (Gutzman and Sive, 2009). Or, an *mypt1* mutant clutch of embryos was treated with 50 μm blebbistatin or 0.1% DMSO at 17 hpf. Embryos were imaged at 19 hpf and then collected and analyzed for genotype following imaging.

Quantitation of neuroepithelial width

Width of the neuroepithelium was measured from the apical midline of one side of the neural tube to the basal edge of the neural tube using 3D doctor (Able Software Corp.). Measurements were taken at the widest region of rhombomere 4 or the r4/r5 boundary. All measurements were done in a single plane of section at a depth located at the apical edge of the developing ear.

RESULTS

A specific sequence of hindbrain ventricle opening

As the brain ventricles form, the closed zebrafish neural tube must separate at the midline and undergo lumen expansion as it fills with eCSF (Lowery and Sive, 2005). In order to determine how these separation and expansion processes occur, we analyzed the temporal sequence of neural tube opening during formation of the hindbrain ventricle. In all vertebrates, the hindbrain neuroepithelium is divided into segmented rhombomeres, transient anteroposterior bulges (Lumsden, 2004; Vaage, 1969), with distinct gene expression and fates. Our focus was on a seven-hour period during zebrafish brain development, 17-24 hours post fertilization (hpf), beginning after completion of neurulation, encompassing the time of initial neural tube opening, neuroepithelial morphogenesis, and ventricle expansion. Emphasis was on the hindbrain, since this forms the largest ventricle. The sequence of hindbrain opening is shown in live embryos, imaged by spinning disk confocal (Fig. 1 and Supplemental Movie 1). At 17 hpf the neural tube has formed a clear midline, and outlines of rhombomeres (r) are apparent as shallow indentations on the outside of the neural tube (Fig. 1A). An initial hindbrain opening was present at approximately 18 hpf, between the boundary of rhombomere 0 (r0) and rhombomere 1 (r1) (Fig. 1B); therefore, we hypothesized that ventricle inflation would occur in an anterior to posterior direction. However, by 19 hpf, when rhombomeres were clearly visible, additional openings appeared at the r3/r4 boundary and the r4/r5 boundary, in the middle of the hindbrain (Fig. 1C). The openings surrounding r4 were consistent with reported r4 determination, as determined by gene

expression, and the sequence of visible rhombomere boundary morphology in the zebrafish (Maves et al., 2002; Moens and Prince, 2002). By 20 hpf, the lumen of the neural tube had begun to open anteriorly and posteriorly from r1, while a new opening was seen at the r2/r3 boundary (Fig. 1D). By 21 hpf, the lumen was open within r2 (Fig. 1E), while by 22 hpf lumen opening was seen within r4, leaving the only visible rhombomere morphology at r3 and r5, the two largest rhombomeres (Fig. 1F). Between 23 and 24 hpf, separation of r3 and r5, occurred and the ventricle lumen expanded (Fig. 1G,H). Thus, by 24 hpf, the neural tube was open with a large ventricular space. The more posterior rhombomeres, r6 and r7, opened in a sequence that was consistent with rhombomere determination by gene expression (data not shown); however, due to the curvature of the embryo, we could not image the entire length of the hindbrain in any one experiment, and focused on more anterior rhombomeres.

These data show that, contrary to our hypothesis, the hindbrain ventricle does not open in an anterior to posterior sequence. Rather, opening occurs in a stereotypical sequence along the length of the hindbrain, with initial openings between rhombomeres, and later coalescence of these openings to form the hindbrain ventricle lumen.

mypt1 mutants have abnormal hindbrain ventricle expansion and retain early rhombomere morphology

In order to define the mechanisms underlying hindbrain ventricle opening and expansion, we focused on the *mypt1*^{hi2653} insertional mutant, identified as having small and abnormally shaped brain ventricles (Amsterdam et al., 2004; Lowery and Sive, unpublished). The retroviral insertion is located in the *mypt1* gene (also called *ppp1r12a*) encoding the protein myosin phosphatase subunit 1 (Mypt1), a required regulator of the

myosin phosphatase holoenzyme (Ito et al., 2004; Matsumura and Hartshorne, 2008) (see Fig. S1 A,B in supplementary material). Gene assignment for *mypt1*^{hi2653} was confirmed by rescue of mutants with wild type *mypt1* mRNA, by RT-PCR for *mypt1* mRNA in mutants (see Fig. S1C,D in supplementary material), and by injection of a *mypt1* splice site morpholino-modified oligonucleotide ("morpholino":MO), and rescue of the phenotype (see Fig. S1E-G in supplementary material). *mypt1* is expressed maternally and zygotically throughout the embryo (see Fig. S2 in supplementary material). The events we describe occur prior to the onset of heartbeat, indicating that circulation is not involved.

In brain ventricles injected with Texas Red dextran (Gutzman and Sive, 2009) at the early stages of hindbrain opening (18-21 hpf), *mypt1* mutants appeared the same as wild type (see Fig. S3 in supplementary material). However, by 24 hpf, *mypt1* mutants had defects in brain structure (Fig. 2A-D), and dorsal images showed that specific regions of the hindbrain remained apposed, without ventricle expansion (Fig. 2A,B). Strikingly, while lateral views showed that rhombomere morphology was not visible in wild type embryos, distinct rhombomeres were visible in *mypt1* mutants (Fig. 2C-F).

The *mypt1* mutant phenotype was examined more closely by high-resolution confocal live imaging at 18, 21, and 24 hpf. Wild type and *mypt1* mutants appeared grossly similar at 18 hpf, although the neural tube was narrower (Fig. 2G,H), while at 21 hpf, hindbrain openings at rhombomere boundaries (r3/r4 and r4/r5) were present in both mutant and wild type, indicating that steps in initial hindbrain opening occurred normally (Fig. 2I,J). However, at 24 hpf, although the neural tube had opened in *mypt1* mutants, the hindbrain ventricle was poorly expanded relative to wild type (Fig. 2K,L'). Consistent

with brightfield imaging, by 24 hpf, wild type embryos had lost distinct rhombomere morphology, whereas in mutants, rhombomere morphology persisted (compare Fig. 2K,K' with Fig. 2L,L').

We excluded the possibility that *mypt1* phenotypes were consequences of changes in cell death or cell proliferation using TUNEL and PH3 staining (see Fig. S4 in supplementary material). In addition, rhombomeric gene expression patterns progressed normally, as did expression of the post-mitotic neuronal marker HuC, in *mypt1* mutants, indicating that the phenotypes are specific to morphogenesis (see Fig. S5 in supplementary material).

The *mypt1* mutant ventricle could have expanded poorly either because too little eCSF was produced, or because the neuroepithelium was incapable of expanding fully. We therefore asked how much the mutant and wild type hindbrain ventricles could be forced to open, by high pressure injection (30psi) of fluid into the ventricle (Fig. 2M). In wild type embryos, hindbrain ventricle width could be increased by 1.5 fold relative to the uninjected ventricle (Fig. 2N and Fig. S6 in supplementary material). However, in mutants, hindbrain ventricle width could be maximally increased by only 1.3 fold relative to its original size. Thus, the *mypt1* mutant neuroepithelium was less able to expand than wild type.

In sum, our data show that in the *mypt1* mutant, a clear hindbrain phenotype is apparent by 24 hpf, after the hindbrain ventricle has opened. Rhombomere morphology does not progress normally, and the hindbrain ventricle is poorly expanded. The data demonstrate that the mutant neuroepithelium is unable to stretch as much as wild type, explaining the small hindbrain ventricle lumen in *mypt1* mutants.

***mypt1* mutants have abnormally shaped neuroepithelial cells**

The persistence of rhombomere morphology in *mypt1* mutants led us to ask whether mutant hindbrain cell shape was abnormal. Scanning confocal imaging at cellular resolution was performed in wild type and mutant embryos at 19 hpf, when the neuroepithelial cells are aligned so that the entire length of the cell can be imaged. At later stages, neuroepithelial cells are tilted and the full length of a cell is difficult to capture. r4, r5 and the r4/r5 boundary were imaged, and 3D cell shapes were reconstructed as described in Methods.

In wild type embryos, cells within the rhombomeres were spindle-shaped that is, narrow apically and basally. In contrast, boundary cells, between rhombomeres, were club shaped: wide at either the apical or basal end and long and narrow at the other (Fig. 3A-C and Fig. S7 in supplementary material). In contrast to wild type, *mypt1* mutant cells within rhombomeres were shorter and wider, and lacked the narrow ends (Fig. 3D-F and Fig. S7 in supplementary material). Cells at the r4/r5 boundary were also shorter and wider, without the characteristic wild type club shape (Fig. 3D-F and Fig. S7 in supplementary material).

Since *mypt1* is broadly expressed, we asked whether the *mypt1* mutant phenotype was a result of activity within the neuroepithelium, or whether surrounding tissues directed the mutant phenotype. In addition, we asked whether the phenotype within the neuroepithelium was cell autonomous. These questions were addressed using transplants of late blastula cells from *mypt1* or control morpholino injected embryos into the presumptive hindbrain region of gastrula stage wild type or *mypt1* embryos (Woo and

Fraser, 1995). Transplanted cells within the hindbrain were assayed for cell shape at 19 hpf. *mypt1* morphant cells transplanted into a control morphant host showed mutant morphology in both intra-rhombomere and rhombomere boundary cells (Figure 3G-I), indicating that Mypt1 functions cell-autonomously in the hindbrain. However, control cells transplanted into *mypt1* morphant hosts adopted *mypt1* mutant cell shapes (Figure 3J-L), demonstrating that wild type cell morphology requires surrounding wild type cells. Consistently, transplants of control cells into control hosts showed wild type cell shapes (Figure 3M-O). In all cases assayed, transplanted cells were present only in the neuroepithelium, and not in epidermal, mesodermal or endodermal cells, indicating that surrounding tissues do not influence neuroepithelial cell shape.

These data show that the characteristic cell shapes within and between wild type rhombomeres are not present in *mypt1* mutants. These abnormalities occur early, before failure of ventricle expansion or failure of rhombomere progression. Wild type cell shape requires a surrounding cohort of wild type cells, whereas mutant cell shape is manifest cell autonomously.

Phosphorylation of myosin regulatory light chain is abnormally elevated and apically localized in the developing brain of *mypt1* mutants

Active myosin phosphatase dephosphorylates myosin regulatory light chain (MRLC) (Ito et al., 2004). Dephosphorylation of MRLC inactivates non-muscle myosin II, and limits contraction (Fig. 4A). Based on this scheme, and knowing that the mutation in Mypt1 would disrupt the binding of Mypt1 and PP1 and render myosin phosphatase inactive, we hypothesized that phosphorylated MRLC (pMRLC) levels would be higher

in *mypt1* mutant brains relative to wild type. The level of pMRLC was examined in brain tissue, microdissected from 18, 21 and 24 hpf embryos (Fig.4B), with or without Mypt1 function. In order to obtain enough brain tissue for analysis by Western blot, we used morpholino injected embryos for these experiments.

At all time points, pMRLC levels were 3-5 fold higher in embryos injected with the *mypt1* MO than in control embryos (Fig. 4C,D). Further, the level of pMRLC in control embryos changed with time, such that pMRLC levels peaked at 21 hpf, and were 2.5-fold lower at 18 hpf and 24 hpf (Fig. 4E). These data show that pMRLC levels change during normal brain development, and that in the *mypt1* mutant, very high levels of pMRLC are present throughout hindbrain ventricle opening.

These changes in pMRLC levels prompted us to ask where pMRLC is localized. Immunocytochemistry was performed on wild type siblings and *mypt1* mutants at 19, 21, and 24 hpf, pMRLC (Fig. 4F-Q). In wild type embryos at 19 hpf, pMRLC was localized on the basal side of the neural tube, with some apical localization, and diffuse expression throughout the cells (Fig. 4F,G). At 21 hpf, pMRLC expression appeared stronger apically, consistent with Western blot data (Fig. 4H,I), and by 24 hpf, apical staining had disappeared (Fig. 4J,K). In *mypt1* mutants, apical pMRLC staining was very strong at all time points assayed (Fig. 4L-Q). Similar to wild type, *mypt1* mutants showed basal pMRLC immunostaining (Fig. 4L-Q).

These data show that, in wild type embryos, phosphorylation of MRLC is dynamic - peaking during neural tube opening and then falling to lower levels as the hindbrain ventricle opens. In contrast, *mypt1* mutants show strongly elevated, apically

localized, pMRLC expression, indicating that Mypt1 regulates both pMRLC levels and localization in the developing brain.

Non-muscle myosin concentrates apically, and both non-muscle myosin II and actin are concentrated at rhombomere boundaries in *mypt1* mutants

Myosin regulatory light chain is bound at the head region of myosin to form the non-muscle myosin II functional unit (Landsverk and Epstein, 2005); therefore, increased apical pMRLC in *mypt1* mutants may lead to apical concentration of non-muscle myosin II (myosin heavy chain). To test this, we performed immunostaining for myosin II on wild type and *mypt1* mutants (Fig. 5). At all stages, myosin II is present basally and within cells. 19 hpf wild type and *mypt1* mutant embryos show a similar pattern of myosin II localization in the brain while at 21 hpf, *mypt1* mutants show slightly increased staining of myosin II at the apical surface of the neuroepithelium compared to wild type (see Fig. S8 supplemental material). However, while in 24 hpf *mypt1* mutants show much stronger apical myosin II staining than wild type (Fig. 5A-C,G-I).

In order to examine the apical surface of the rhombomeres more closely, we removed the roofplate and flat mounted the neural tube (see diagram Fig. 5F). Strikingly, in *mypt1* mutants, but not in wild type, myosin II staining was present at the rhombomere boundaries, in a line along the apical surfaces of boundary cells (Fig. 5D, arrows in Fig. 5E). This staining was consistent with persistence of rhombomere morphology in *mypt1* mutants.

We also analyzed localization of actin, another critical component of the cytoskeleton, which interacts with myosin (Lecuit and Lenne, 2007). In wild type

embryos, actin surrounded cells and was concentrated at the apical cell surfaces lining the brain ventricle, consistent with actin localization at adherens junctions (Fig. 5J,M and diagrams in L,O). The levels and apical localization of actin did not appear altered in *mypt1* mutants (Fig. 5N). However, dorsal 3D projection views of *mypt1* mutant embryo hindbrain showed strong accumulation of actin at rhombomere boundaries (arrows Fig. 5K), consistent with myosin II localization.

These data indicate that in *mypt1* mutants, non-muscle myosin II, along with pMRLC, is concentrated apically in the hindbrain neuroepithelium. Non-muscle myosin II and actin are abnormally localized at rhombomere boundaries, suggesting that this may be responsible for failure of rhombomere morphology progression.

Abnormal ventricle morphogenesis in *mypt1* mutants is myosin dependent

We used an independent approach to ask whether over active myosin was responsible for the *mypt1* mutant phenotype, asking whether the myosin II inhibitor, blebbistatin (Kovacs et al., 2004) would rescue the hindbrain ventricle phenotype (Fig. 6A,B). At 22 hpf, mutant or wild type embryos were treated with DMSO as a control, or 50 μm blebbistatin. After 3 hours of treatment, embryos were ventricle injected and then imaged (Fig. 6C-J). Blebbistatin slightly reduced the size of the wild type hindbrain ventricle (Fig. 6E,F), but did not alter rhombomere morphology. However, blebbistatin treatment fully rescued the *mypt1* mutant phenotype (Fig. 6I,J), with the hindbrain ventricle fully open, and rhombomere morphology no longer apparent. Other phenotypes in the mutant embryo were also rescued, including the abnormal notochord and somites (Fig. 6G,H). Additionally, the inability of *mypt1* mutant neuroepithelium to fully expand

when forced open with high pressure injection (Fig. 2N) was also rescued by blebbistatin treatment (see Fig. S9 in supplementary material). These data confirm that the *mypt1* phenotype is a result of overactive myosin contraction, and that myosin II inactivation is required for hindbrain morphogenesis and full ventricle expansion.

mypt1 neuroepithelial cells are abnormally shaped due to myosin contraction

We extended this analysis (Fig. 3) to ask whether blebbistatin would correct mutant cell shape. A *mypt1* mutant clutch of embryos was injected with memGFP mRNA and treated with 50 μm blebbistatin at 17 hpf. At 19hpf, embryos were imaged, and 3D cell shapes were reconstructed. Since the mutant phenotype is not grossly visible at this time, embryos were genotyped by PCR (Fig. 7A). *mypt1* mutants treated from 17 hpf to 19 hpf with blebbistatin showed normal cell shapes within and between rhombomeres (compare Fig. 7c,d and g,h).

As a corollary to cell shape changes, we quantified the width of the neuroepithelium in all treatment groups, by measuring the distance from the apical side of the epithelium to the basal side at r4 and at the r4/r5 boundary. In *mypt1* mutants, tube width was significantly (13%) narrower than in wild type embryos at r4 and at the r4/r5 boundary (10%) (Fig. 7C and Fig. S10 in supplementary material). In *mypt1* mutants treated with blebbistatin, neural tube width was restored to the wild type width (Fig. 7C and Fig. S10 in supplementary material).

These data demonstrate that hindbrain cell shape and neural tube width, is regulated by myosin activity.

DISCUSSION

Cell shape, rhombomere morphogenesis and ventricle expansion are regulated by myosin contractility

We demonstrate for the first time, that modulation of myosin activity by myosin phosphatase affects three aspects of normal hindbrain development: neuroepithelial cell shape, morphogenesis of the rhombomeres and expansion of the hindbrain ventricle (Fig. 8). Of particular significance is our finding that, unless myosin contractility is reduced, the lumen of the neural tube cannot expand to form the normal hindbrain ventricle.

Regulation of neuroepithelial cell shape via apical modulation of myosin function

The earliest hindbrain phenotype we observed in *mypt1* mutants was abnormal cell shape. Spindle shaped rhombomeric cells and club-shaped boundary cells lost their characteristic shapes with inhibition of *mypt1* and overactive myosin. It is not clear what normally drives formation of these disparate shapes; however, cells within rhombomeres are more adhesive than those between (Cooke et al., 2005), perhaps contributing to cell shape differences. Mosaic analysis showed that *mypt1* mutant cells always assumed mutant shape, regardless of the genotype of the surrounding cells, indicating cell autonomous Mypt1 function. However, wild type cell shape required that surrounding cells also be wild type, suggesting a non-autonomous function. One possible explanation for these results is that wild type cells cannot push or pull enough against the stiff *mypt1* neuroepithelium to realize their normal shapes. Another possibility is that wild type cells must be fully connected through junctions in the epithelial sheet in order to undergo

correct shape change. Interestingly, a similar duality of cell-autonomous and non-autonomous phenotype was also observed for *mypt1* function during convergent extension (Weiser et al., 2009)

Loss of asymmetric shape in cells with overactive myosin raises the question of whether Mypt1 acts through the apical or basal side of the cell. In embryos lacking *mypt1* function, the pMRLC was concentrated at the apical surface of the neuroepithelium. Since the strong expression of pMRLC and myosin II basally appeared unaltered after *mypt1* loss of function, the effects of Mypt1 are likely mediated through the apical side of the epithelium.

Consistent with regulation of cell shape via apical myosin activity, Kinoshita et al. demonstrated Rho localization at the apical surface of the epithelium during chick neurulation, and connected some of its effects with pMRLC (Kinoshita et al., 2008). In the developing *Drosophila* eye, myosin II regulates changes in both cell shape and cell clustering, and in *spaghetti squash* (MRLC mutant) and *zipper* (myosin heavy chain mutant) the apical surface does not constrict (Escudero et al., 2007; Hildebrand, 2005; Lee and Treisman, 2004).

Sequence of hindbrain opening, and rhombomere progression

A later phenotype in the *mypt1* mutant was failure of rhombomeres to progress through their normal sequence of morphogenesis, whereby rhombomere morphology is lost over the six-hour time period we analyzed. This progression is dependent on inhibition of myosin activity, and coupled to the normal dynamic changes in pMRLC levels, which peak as the neural tube midline separates, and decrease as rhombomere

morphology progresses. During the time period when rhombomere morphology would normally have been lost, in the *mypt1* mutant, myosin II and actin were strongly concentrated at rhombomere boundaries, and not visible at wild type boundaries. Thus, an overactive actinomyosin network at the rhombomere boundaries in the *mypt1* mutant may hold the rhombomeres in their morphologically segmented state.

Failure of morphological rhombomere progression in *mypt1* mutants was independent of the changes in gene expression characteristic of differentiating rhombomeres, indicating that morphology, and not cell type determination, is under actinomyosin regulation. This failure of rhombomere progression is also independent of fluid pressure within the ventricle space as *snakehead* mutants lacking embryonic cerebrospinal fluid do not have arrested rhombomere morphology (Lowery and Sive, 2005). Further, the *mypt1* phenotype did not involve control of cell number, since neither cell proliferation, nor cell death was affected, further pointing to myosin contractility as the major player in this morphogenetic change.

"Epithelial relaxation" and the role of myosin in ventricle expansion

Opening of the hindbrain ventricle along the neural tube midline begins normally in *mypt1* mutants, but later, the ventricle does not expand completely as a result of a "stiff" mutant neuroepithelium.

In many organs (for example, McCray et al., 1992), tubes initially form without a lumen, or with only a small lumen, which must expand to allow the tube to function. Part of this expansion is through fluid secretion, and in the embryonic brain, the ventricular lumen expands as it fills with eCSF (Lowery and Sive, 2009). However, this study shows

that ventricular lumen expansion also requires a stretchy neuroepithelium, which can expand appropriately with eCSF. We have coined the term "epithelial relaxation" to describe the acquisition of stretchiness, which depends upon inhibition of myosin contractility, and suggest that this may be a widespread mechanism underlying expansion of epithelial tubes in other organs.

How would myosin activity regulate cell stretching, or elasticity? Elasticity of a cell is determined by the cytoskeleton, primarily through the cortical actinomyosin network. Cortical tension is created when myosin II contracts, pulling actin filaments together (Clark et al., 2007). In *mypt1* mutants, cortical actin localization does not change, except at rhombomere boundaries, but the excessive myosin contraction would increase cytoskeletal tension in all cells, resulting in a more rigid, less "stretchy" cell, and a less elastic neuroepithelium. Our data complement the observation that earlier, myosin is required for neural plate stiffness during neurulation in *Xenopus* (Rolo et al., 2009). After neurulation, myosin function must be suppressed to increase stretchiness of the neuroepithelium, enabling the hindbrain ventricle to expand.

Another consideration is that, because cells are connected by junctions, the neuroepithelium may act as a unit during morphogenesis and ventricle formation (Lowery and Sive, 2009). In tissue culture cells, Mypt1 interacts with ERM proteins in the apical junction complex (Eto et al., 2005; Kawano et al., 1999), suggesting that apical junctions may be abnormal in the *mypt1* mutant. However, immunostaining with several apical junction markers showed no abnormalities in the mutants described here (Figure 5 and data not shown).

Epithelial relaxation has not previously been described during development, but may be similar to the changes in contraction and relaxation of tubes that are surrounded by smooth muscle. Like non-muscle myosin, smooth muscle is also regulated by Mypt1 and myosin phosphatase (Pfitzer, 2001), and, processes akin to epithelial relaxation may exist in vascular smooth muscle (Hirano, 2007), smooth muscle of the urinary bladder (Ding et al., 2009; Poley et al., 2008), gastrointestinal smooth muscle (Huang et al., 2005; Ihara et al., 2007), and secretion of bile by the gall bladder (Camello-Almaraz et al., 2009).

Is there a connection between all *mypt1* hindbrain phenotypes?

Downstream of myosin function, it is not clear whether each of the events described is under the same molecular control, and whether one of these events affects another. For example, cell shape abnormalities are the earliest phenotypes we observe in the *mypt1* mutant. Do these abnormally shaped cells contribute to a failure of rhombomere morphology progression, or to failure of the hindbrain ventricle to expand? Since myosin II and actin accumulated at rhombomere boundaries, excess contraction along a line of boundary cells, in effect functioning as a unit, may prevent progression of rhombomere morphogenesis. Thus, rhombomere progression may correlate with abnormally shaped cells, but may not be caused by the abnormal cell shape, per se. With regard to ventricle opening, we believe it is most relevant to view this process as a result of epithelial sheet activity, rather than as dependent on individual cell shape. However, *mypt1* mutant cells may be more rigid than wild type cells, and, as a group, may contribute to epithelial "tightness" and failure of hindbrain ventricle expansion. Are

rhombomere progression and ventricle opening linked? In wild type embryos, rhombomere progression and ventricle expansion both occur as pMRLC levels decline, but it is unclear whether these events are interdependent. Future studies will focus on additional mechanisms underlying epithelial relaxation, the connection between the events described here, and the regulation of *mypt1* activity in the neuroepithelium.

ACKNOWLEDGEMENTS

We thank our colleagues for useful criticism, particularly, Amanda Dickinson, Alena Shkumatava and Ellie Graeden. We thank Olivier Paugois for expert fish husbandry, and Nancy Hopkins and Adam Amsterdam for the kind gift of the *mytp1*^{hi2364} fish line. Many thanks to Paul Mastsudaira and James Evans for advice and tuition in imaging. This work was conducted using the Whitehead-MIT Bioimaging Center and the W. M. Keck Foundation Biological Imaging Facility at the Whitehead Institute. HS is supported by NIH. JHG is supported by an MIT CSBi/Merck postdoctoral fellowship.

REFERENCES

Amsterdam, A., Nissen, R. M., Sun, Z., Swindell, E. C., Farrington, S. and Hopkins, N. (2004). Identification of 315 genes essential for early zebrafish development. *Proc Natl Acad Sci U S A* **101**, 12792-7.

Camello-Almaraz, C., Macias, B., Gomez-Pinilla, P. J., Alcon, S., Martin-Cano, F. E., Baba, A., Matsuda, T., Camello, P. J. and Pozo, M. J. (2009). Developmental

changes in Ca2+ homeostasis and contractility in gallbladder smooth muscle. *Am J Physiol Cell Physiol* **296**, C783-91.

Clark, K., Langeslag, M., Figdor, C. G. and van Leeuwen, F. N. (2007). Myosin II and mechanotransduction: a balancing act. *Trends Cell Biol* **17**, 178-86.

Cooke, J. E., Kemp, H. A. and Moens, C. B. (2005). EphA4 is required for cell adhesion and rhombomere-boundary formation in the zebrafish. *Curr Biol* **15**, 536-42.

Ding, H. L., Ryder, J. W., Stull, J. T. and Kamm, K. E. (2009). Signaling processes for initiating smooth muscle contraction upon neural stimulation. *J Biol Chem* **284**, 15541-8.

Escudero, L. M., Bischoff, M. and Freeman, M. (2007). Myosin II regulates complex cellular arrangement and epithelial architecture in Drosophila. *Dev Cell* **13**, 717-29.

Eto, M., Kirkbride, J. A. and Brautigan, D. L. (2005). Assembly of MYPT1 with protein phosphatase-1 in fibroblasts redirects localization and reorganizes the actin cytoskeleton. *Cell Motil Cytoskeleton* **62**, 100-9.

Gato, A. and Desmond, M. E. (2009). Why the embryo still matters: CSF and the neuroepithelium as interdependent regulators of embryonic brain growth, morphogenesis and histiogenesis. *Dev Biol* **327**, 263-72.

Gutzman, J. H., Graeden, E. G., Lowery, L. A., Holley, H. S. and Sive, H. (2008). Formation of the zebrafish midbrain-hindbrain boundary constriction requires laminin-dependent basal constriction. *Mech Dev* **125**, 974-83.

Gutzman, J. H. and Sive, H. (2009). Zebrafish brain ventricle injection. *Journal of Visualized Experiments*, http://www.jove.com/index/details.stp?id=1218, doi: 10.3791/1218.

Hanneman, E., Trevarrow, B., Metcalfe, W. K., Kimmel, C. B. and Westerfield, M. (1988). Segmental pattern of development of the hindbrain and spinal cord of the zebrafish embryo. *Development* **103**, 49-58.

Hartshorne, D. J., Ito, M. and Erdodi, F. (2004). Role of protein phosphatase type 1 in contractile functions: myosin phosphatase. *J Biol Chem* **279**, 37211-4.

Heyman, I., Kent, A. and Lumsden, A. (1993). Cellular morphology and extracellular space at rhombomere boundaries in the chick embryo hindbrain. *Dev Dyn* **198**, 241-53.

Hildebrand, J. D. (2005). Shroom regulates epithelial cell shape via the apical positioning of an actomyosin network. *J Cell Sci* **118**, 5191-203.

Hirano, K. (2007). Current topics in the regulatory mechanism underlying the Ca2+ sensitization of the contractile apparatus in vascular smooth muscle. *J Pharmacol Sci* **104**, 109-15.

Huang, H., Ruan, H., Aw, M. Y., Hussain, A., Guo, L., Gao, C., Qian, F., Leung, T., Song, H., Kimelman, D. et al. (2008). Mypt1-mediated spatial positioning of Bmp2-producing cells is essential for liver organogenesis. *Development* **135**, 3209-18.

Huang, J., Zhou, H., Mahavadi, S., Sriwai, W., Lyall, V. and Murthy, K. S. (2005). Signaling pathways mediating gastrointestinal smooth muscle contraction and MLC20 phosphorylation by motilin receptors. *Am J Physiol Gastrointest Liver Physiol* **288**, G23-31.

Ihara, E., Moffat, L., Ostrander, J., Walsh, M. P. and MacDonald, J. A. (2007). Characterization of protein kinase pathways responsible for Ca2+ sensitization in rat ileal longitudinal smooth muscle. *Am J Physiol Gastrointest Liver Physiol* **293**, G699-710.

Ito, M., Nakano, T., Erdodi, F. and Hartshorne, D. J. (2004). Myosin phosphatase: structure, regulation and function. *Mol Cell Biochem* **259**, 197-209.

Kawano, Y., Fukata, Y., Oshiro, N., Amano, M., Nakamura, T., Ito, M., Matsumura, F., Inagaki, M. and Kaibuchi, K. (1999). Phosphorylation of myosin-binding subunit (MBS) of myosin phosphatase by Rho-kinase in vivo. *J Cell Biol* **147**, 1023-38.

Kimmel, C. B., Ballard, W. W., Kimmel, S. R., Ullmann, B. and Schilling, T. F. (1995). Stages of embryonic development of the zebrafish. *Dev Dyn* **203**, 253-310.

Kinoshita, N., Sasai, N., Misaki, K. and Yonemura, S. (2008). Apical accumulation of rho in the neural plate is important for neural plate cell shape change and neural tube formation. *Mol Biol Cell* **19**, 2289-99.

Kovacs, M., Toth, J., Hetenyi, C., Malnasi-Csizmadia, A. and Sellers, J. R. (2004). Mechanism of blebbistatin inhibition of myosin II. *J Biol Chem* **279**, 35557-63.

Landsverk, M. L. and Epstein, H. F. (2005). Genetic analysis of myosin II assembly and organization in model organisms. *Cell Mol Life Sci* **62**, 2270-82.

Lecuit, T. and Lenne, P. F. (2007). Cell surface mechanics and the control of cell shape, tissue patterns and morphogenesis. *Nat Rev Mol Cell Biol* **8**, 633-44.

Lee, A. and Treisman, J. E. (2004). Excessive Myosin activity in mbs mutants causes photoreceptor movement out of the Drosophila eye disc epithelium. *Mol Biol Cell* **15**, 3285-95.

Lowery, L. A., De Rienzo, G., Gutzman, J. H. and Sive, H. (2008). Characterization and Classification of Zebrafish Brain Morphology Mutants. *Anat Rec* **292**, 94-106.

Lowery, L. A. and Sive, H. (2005). Initial formation of zebrafish brain ventricles occurs independently of circulation and requires the nagie oko and snakehead/atp1a1a.1 gene products. *Development* **132**, 2057-67.

Lowery, L. A. and Sive, H. (2009). Totally tubular: the mystery behind function and origin of the brain ventricular system. *Bioessays* 31, 446-58.

Lumsden, A. (2004). Segmentation and compartition in the early avian hindbrain. *Mech Dev* **121**, 1081-8.

Matsumura, F. and Hartshorne, D. J. (2008). Myosin phosphatase target subunit: Many roles in cell function. *Biochem Biophys Res Commun* **369**, 149-56.

Maves, L., Jackman, W. and Kimmel, C. B. (2002). FGF3 and FGF8 mediate a rhombomere 4 signaling activity in the zebrafish hindbrain. *Development* **129**, 3825-37.

McCray, P. B., Jr., Bettencourt, J. D. and Bastacky, J. (1992). Developing bronchopulmonary epithelium of the human fetus secretes fluid. *Am J Physiol* **262**, L270-9.

Mizuno, T., Tsutsui, K. and Nishida, Y. (2002). Drosophila myosin phosphatase and its role in dorsal closure. *Development* **129**, 1215-23.

Moens, C. B. and Prince, V. E. (2002). Constructing the hindbrain: insights from the zebrafish. *Dev Dyn* **224**, 1-17.

Pfitzer, G. (2001). Invited review: regulation of myosin phosphorylation in smooth muscle. *J Appl Physiol* **91**, 497-503.

Poley, R. N., Dosier, C. R., Speich, J. E., Miner, A. S. and Ratz, P. H. (2008). Stimulated calcium entry and constitutive RhoA kinase activity cause stretch-induced detrusor contraction. *Eur J Pharmacol* **599**, 137-45.

Quintin, S., Gally, C. and Labouesse, M. (2008). Epithelial morphogenesis in embryos: asymmetries, motors and brakes. *Trends Genet* **24**, 221-30.

Rolo, A., Skoglund, P. and Keller, R. (2009). Morphogenetic movements driving neural tube closure in Xenopus require myosin IIB. *Dev Biol* **327**, 327-38.

Tan, C., Stronach, B. and Perrimon, N. (2003). Roles of myosin phosphatase during Drosophila development. *Development* **130**, 671-81.

Vaage, S. (1969). The segmentation of the primitive neural tube in chick embryos (Gallus domesticus). A morphological, histochemical and autoradiographical investigation. *Ergeb Anat Entwicklungsgesch* **41**, 3-87.

Watanabe, T., Hosoya, H. and Yonemura, S. (2007). Regulation of myosin II dynamics by phosphorylation and dephosphorylation of its light chain in epithelial cells. *Mol Biol Cell* **18**, 605-16.

Weiser, D. C., Row, R. H. and Kimelman, D. (2009). Rho-regulated Myosin phosphatase establishes the level of protrusive activity required for cell movements during zebrafish gastrulation. *Development* **136**, 2375-84.

Westerfield, M. (1995). The Zebrafish Book: A guide for the laboratory use of zebrafish.: University of Oregon Press.

Woo, K. and Fraser, S.E. (1995). Order and coherence in the fate map of the zebrafish nervous system. *Development* **121,** 2595-2609.

Xia, D., Stull, J. T. and Kamm, K. E. (2005). Myosin phosphatase targeting subunit 1 affects cell migration by regulating myosin phosphorylation and actin assembly. *Exp Cell Res* **304**, 506-17.

FIGURE LEGENDS

Fig. 1. The sequence of wild type hindbrain ventricle opening. (**A-H**) Time course of wild type hindbrain ventricle opening from 17 hpf to 24 hpf. Embryos were injected with memGFP mRNA (n=12). Model images are a representative snapshot of the hindbrain opening at each time point. (A) 17 hpf, the neural tube is closed with visible rhombomere morphology. (B) 18 hpf, the initial opening is visible at the r0/r1 boundary. (C) 19 hpf, openings surrounding r4 are visible. (D) 20 hpf, there are openings at the r2/r3 boundary and r1 has separated completely. (E) 21 hpf, opening within r2 occurs. (F) 22 hpf, separation within r4 has occurred. (G) 23 hpf, separation within r3 has occurred. (H) 24 hpf, separation within r5 occurs resulting in an open ventricle and less prominent rhombomere morphology. Asterisks denote the ear. Arrowheads indicate regions that are separating. r0-r5 indicate specific rhombomeres. Anterior is to the left**.**

Fig. 2. *mypt1* mutant phenotype. (**A-F**) 24 hpf wild type and *mypt1* mutant brain ventricle injections. Wild type (A) and *mypt1* (B) dorsal views. Wild type (C) and *mypt1* (D) lateral views. (**E-F**) Higher magnification of boxed region in C and D respectively. Arrowheads indicate rhombomere boundaries. (**G-L'**) Live confocal imaging of the hindbrain in wild type (G,I,K,K') and *mypt1* mutants (H,J,L,L') after memGFP mRNA injection. (G,H) 18 hpf, wild type and *mypt1* mutants respectively. (I,J) 21 hpf, wild type and *mypt1* mutant respectively with similar morphology and hindbrain openings (see arrows). (K,L) 24 hpf wild type and *mypt1* mutant respectively. (K'-L') are the same image as in K and L respectively with neuroepithelial tissue outlined in yellow. Dotted lines denote rhombomere morphology (L') (n>10 for all panels). *mypt1* mutants have a

normal neural tube, suggesting maternal gene expression is sufficient for brain development until the end of neurulation. Consistent with this, inhibition of Mypt1 expression using a start site MO led to a disorganized neural tube (data not shown), whereas a splice site MO (see Fig. S1 in supplementary material) showed a phenotype only after the neural tube had formed. **(M)** Schematic of the hindbrain "before" and at "maximum" forced ventricle expansion, **a** and **b** indicate regions that were measured. **(N)** Quantitation of the expandability of the hindbrain neuroepithelium in wild type and *mypt1* mutants. Two independent experiments were averaged, wt n=12, *mypt1* n=15. Data are represented as an Expansion Ratio +/- standard deviation. Bars are significantly different using the Mann-Whitney U test $p<0.001$. Asterisks denote the ear. r0-r5 label specific rhombomeres. Anterior is to the left. H=hindbrain ventricle. Scale bars A-F=100μm, G-L'=50μm.

Fig. 3. Abnormal cell shape in *mypt1* mutants and cell shape mosaic analysis. (A-F) Wild type and *mypt1* mutant embryos injected with memGFP mRNA and confocal imaged. Single cells were traced through a z-series then reconstructed in 3D. (**A**) 19 hpf wild type embryo. (**B**) Same image as in A with three cells outlined shown in one z-plane. (**C**) 3D shape of the cells shown in panel B. (**D**) 19 hpf *mypt1* mutant embryo. (**E**) Same image as in D with three cells outlined shown in one z-plane. (**F**) 3D shapes of cells shown in panel E. Rhombomeres are outlined in yellow dotted lines and boundary cells are visible between rhombomeres (A,D). Red=dividing cell, yellow=rhombomere cell, blue=boundary cell. Wild type and *mypt1* mutant dividing cells were similar in shape. Each image is representative from 3 independent experiments, at least 3 embryos were

imaged and 3-5 cells were reconstructed in 3D for each embryo, per experiment. **(G-O)** Wild type embryos were injected with control MO or *mypt1* MO and memCherry or memGFP mRNA as indicated. Cells were transplanted from the memGFP injected donors to memCherry injected hosts. Transplanted embryos were imaged at 19 hpf by scanning confocal microscopy. **(G-H)** Control MO injected host (red) with *mypt1* MO donor cells (green). **(I)** 3D shape of transplanted donor cells. **(J-K)** *mypt1* MO injected hosts (red) with control MO donor cells (green). **(L)** 3D shape of transplanted donor cells. **(M-N)** Control MO injected host (red) with control MO donor cells (green). **(O)** 3D shape of transplanted donor cells. Cells were reconstructed in 3D using Imaris. Rhombomeres are outlined in yellow (G,J,M) Each image is representative of at least 3 independent experiments where at least 3 embryos were imaged. 3 or more cells were reconstructed in 3D for each embryo per experiment. Scale bars=25μm.

Fig. 4. pMRLC is abnormally elevated and persists apically in the developing brain of *mypt1* mutants. **(A)** Model of Mypt1 as part of myosin phosphatase. **(B)** Hypothesis model for *mypt1* mutant myosin phosphatase. **(C)** Western blot of brain tissue dissected from embryos at 18, 21, and 24 hpf after injection with control MO or *mypt1* splice site MO with actin control. Approximately 100 brains were dissected for each treatment group and 50μg of protein was analyzed. **(D)** Quantitation of fold changes of pMRLC normalized to actin at 18 hpf comparing control MO injected to *mypt1* MO injected embryos. Three independent experiments. **(E)** Quantitation of fold changes of pMRLC normalized to actin over time in control MO embryos. Three independent experiments. **(F-Q)** Transverse vibratome sections through the hindbrain of embryos stained with

pMRLC (green), and counterstained nuclei with propidium iodide (red). Representative images from 4 independent experiments, 2-3 embryos were imaged at each stage per experiment. (F) Wild type embryo at 19 hpf. (G) Higher magnification of the region indicated in F. (H) Wild type embryo at 21 hpf. (I) Higher magnification of the region indicated in H. (J) Wild type embryo at 24 hpf. (K) Higher magnification of the region indicated in J. (L) *mypt1* mutant embryo at 19 hpf. (M) Higher magnification of the region indicated in L. (N) *mypt1* mutant embryo at 21 hpf. (O) Higher magnification of the region indicated in N. (P) *mypt1* mutant at 24 hpf. (Q) Higher magnification of the region indicated in P. Dorsal is to the top. Arrows point to the apical neuroepithelial surface in all images. F,H,J,L,N,P scale bars=50μM; G,I,K,M,O,Q scale bars=10μM.

Fig. 5. Abnormal localization of non-muscle myosin II and actin in *mypt1* mutants. **(A-I)** Wild type and *mypt1* mutant embryos were stained with non-muscle myosin II antibody (green) and counterstained with propidium iodide to label nuclei (red). Representative images from 4 independent experiments. For each experiment 2-3 embryos were imaged. **(A-B)** 3D projection of a whole mount wild type (A) or *mypt1* mutant (B) at 24 hpf. **(C)** Diagram of region imaged in A and B. **(D-E)** Wild type (D) and *mypt1* mutant (E) at 24 hpf mounted after removal of the roof plate imaging the region shown in the small box in A labeled D' (wild type) or in B labeled E' (*mypt1* mutant). **(F)** Diagram of region imaged in D and E. **(G-H)** Vibratome section of a 24 hpf wild type (G) or *mypt1* mutant (H) embryo. **(I)** Region of the embryo sectioned for G and H. **(J-O)** Wild type and *mypt1* mutants stained with phalloidin (green). Representative images from 2 independent experiments. For each experiment 3-4 embryos were imaged. **(J-K)**

3D projection of a whole mount wild type (J) or *mytp1* mutant (K) at 24 hpf. **(L)** Diagram of region imaged in J and K. **(M-N)** Vibratome section of a wild type (M) or *mypt1* mutant (N) embryo at 24 hpf. **(O)** Diagram of embryo stage and region imaged in M and N. Scale bars=50μM for A-B, G-H, J-K, M-N. Scale bars=25 μM for D-E.

Fig. 6. Abnormal rhombomere progression and ventricle expansion in *mypt1* mutants is myosin dependent. (A) Schematic for blebbistatin rescue of the *mypt1* mutant phenotype. **(B)** Experimental outline. Embryos from an *mypt1* heterozygous cross were sorted at 20 hpf based on an early notochord and somite phenotype in *mypt1* mutants (J. Gutzman, unpublished data). After DMSO control or blebbistatin treatments, brains were ventricle injected and imaged. Representative images from 3 independent experiments. **(C,D)** Dorsal and lateral images of a wild type embryo treated with DMSO control, 100% of the embryos looked wild type (n=56/56). **(E,F)** Dorsal and lateral images of a wild type embryo treated with 50μM blebbistatin. 45% resulted in a slightly less inflated ventricle (n=36/80), but all still had normal brain morphology. **(G,H)** *mypt1* mutant embryo treated with DMSO, 100% had the mutant phenotype (n=22/22). **(I,J)** *mypt1* mutant rescued with blebbistatin, 79% of mutants were rescued (n=33/42). Asterisks denote the ear. Anterior is to the left.

Fig. 7. Abnormal cell shape in *mypt1* mutants and rescue with myosin II inhibitor. (A) Experimental outline for blebbistatin rescue of cell shape in *mypt1* mutants. 1. Injection of memGFP mRNA into *mypt1* mutant clutch. 2. 17 hpf embryos treated with 0.1% DMSO or 50μm blebbistatin. 3. Live imaging of the hindbrain by scanning

confocal microscopy. 4. PCR identification of wild type and *mypt1* mutant embryos imaged. **(B)** Blebbistatin rescue results. **(a)** Wild type embryo treated with DMSO, cells were outlined and **(e)** 3D reconstructed. **(b)** Wild type embryo treated with blebbistatin, cells were outlined and **(f)** 3D reconstructed. **(c)** *mypt1* mutant treated with DMSO, cells were outlined and **(g)** 3D reconstructed. **(d)** *mypt1* mutant treated with blebbistatin, cells were outlined and **(h)** 3D reconstructed. Images are representative from 3 independent experiments. At least 4 embryos for each treatment group were analyzed for cell shape, 3-5 cells were outlined from each embryo. **(C)** Quantitation of neural tube width at the widest region of r4 (or the boundary between r4/r5, Fig. S9 in supplemental material) in embryos treated with DMSO or blebbistatin as indicated. (wild type+DMSO n=7, wild type+bleb n=8, *mypt1*+DMSO n=6, *mypt1*+bleb n=5). r4, r5 indicate rhombomere number. Yellow=rhombomere cells, blue=boundary cells. Asterisks denote the ear. Anterior is to the left. In C, asterisks indicates that the bar is significantly different from all other bars using the Mann-Whitney U test, $p<0.01$. Scale bars=25μM.

Fig. 8. Model for the requirement of *mypt1* in the regulation of myosin during brain morphogenesis. Proposed requirements for Mypt1 during zebrafish brain morphogenesis. Mypt1 is required for proper rhombomeric cell shape at 19 hpf. It is also required later for progression of rhombomere morphology and for brain ventricle expansion. The requirement for Mypt1 during formation of rhombomere morphology and during ventricle opening is unclear; however, our data suggest that myosin may be required for these earlier steps, which would indicate that Mypt1 inhibition of myosin phosphatase may be required during those processes.

Figure 1.

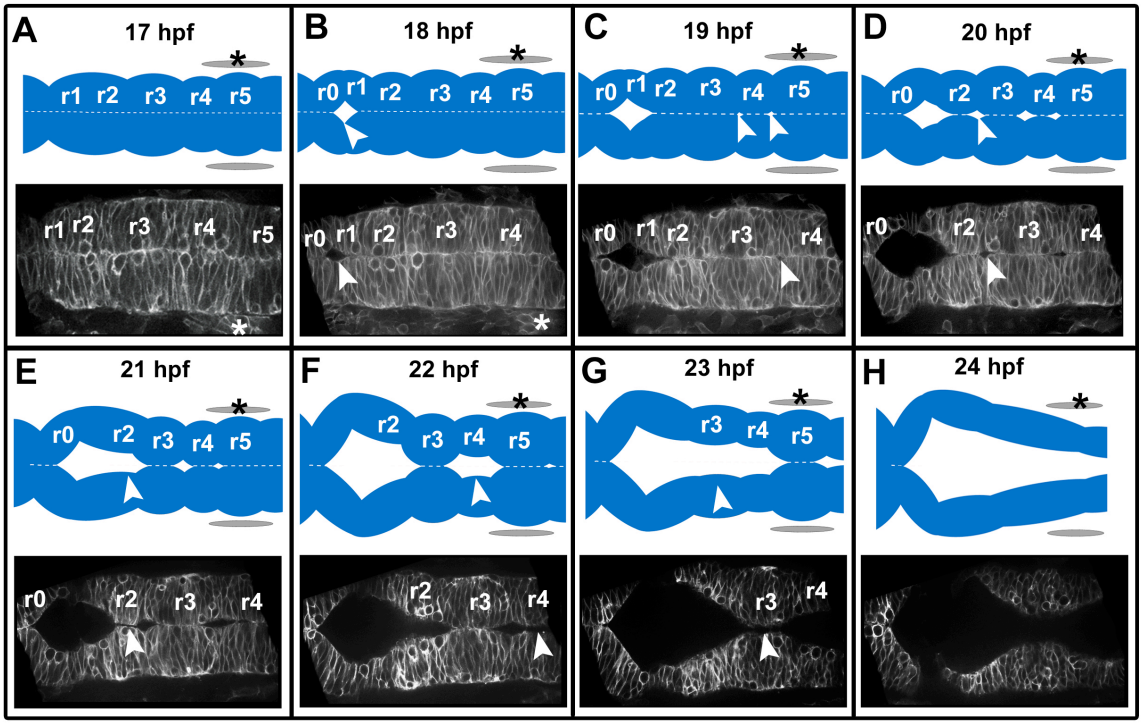

Figure 2.

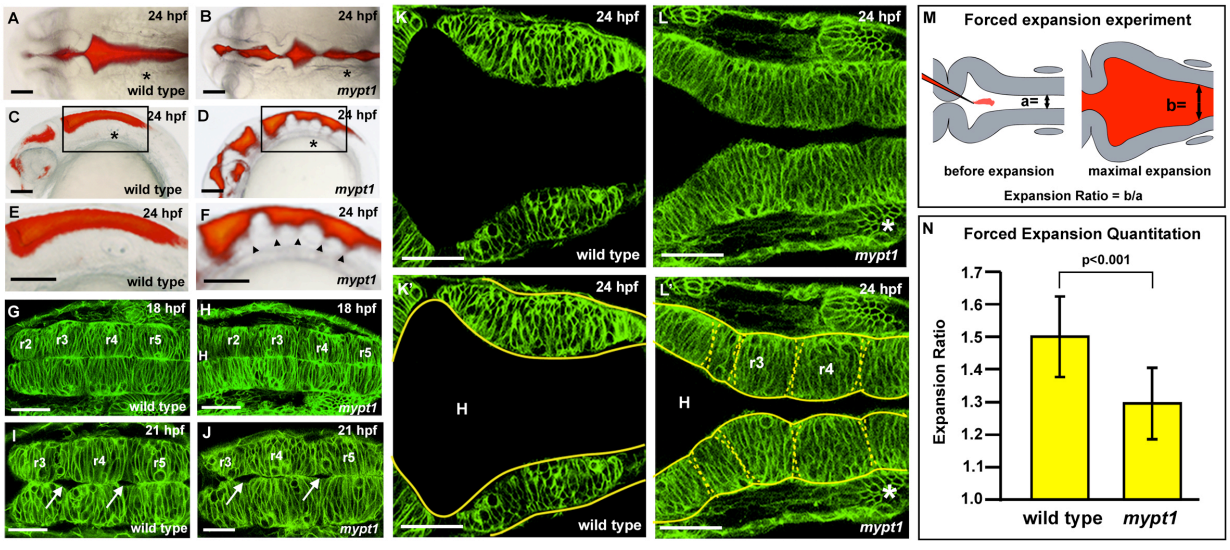

Figure 3.

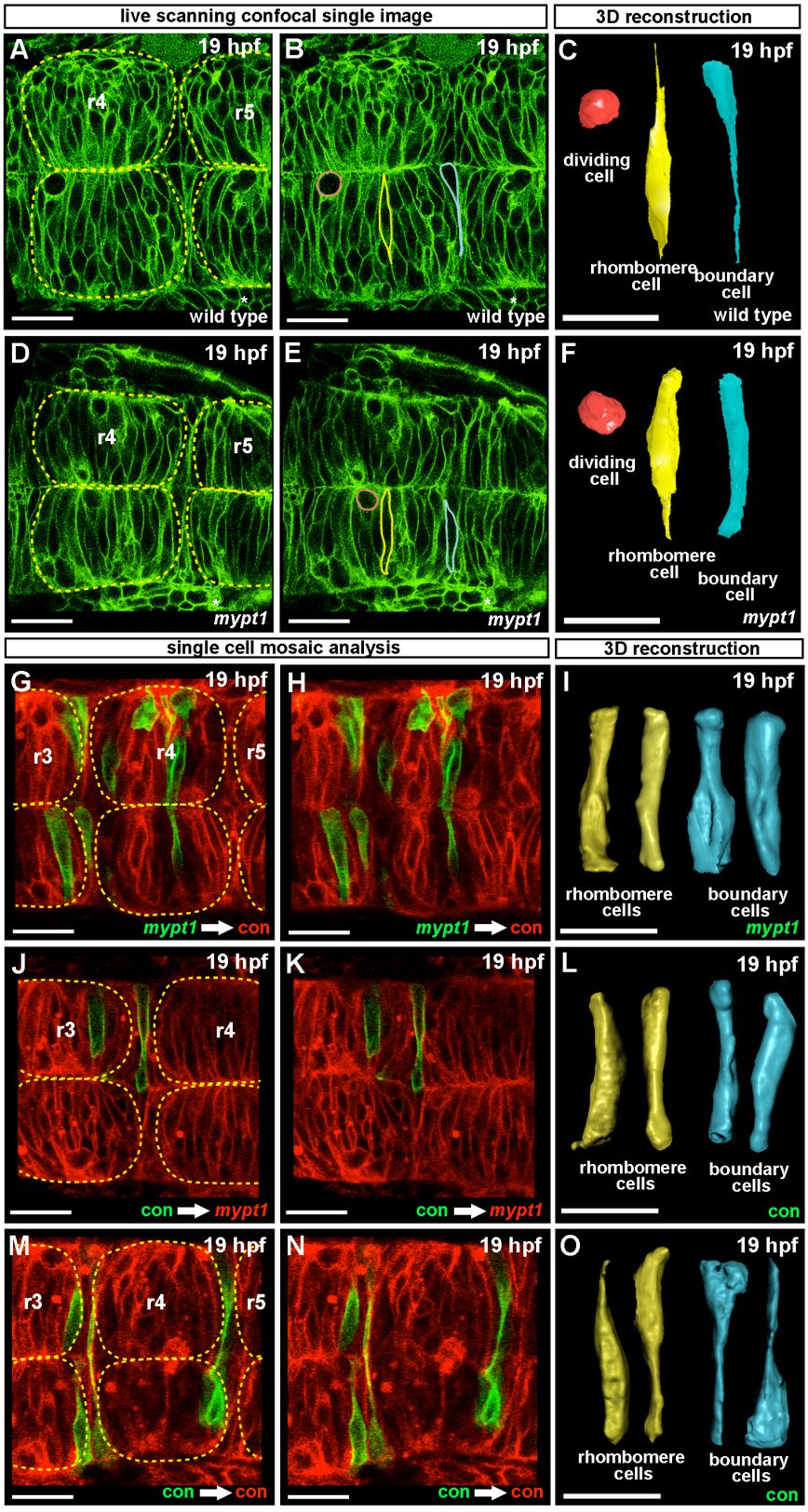
live scanning confocal single image
3D reconstruction
A
19 hpf
r4
r5
wild type
B
19 hpf
wild type
C
19 hpf
dividing cell
rhombomere cell
boundary cell
wild type
D
19 hpf
r4
r5
mypt1
E
19 hpf
mypt1
F
19 hpf
dividing cell
rhombomere cell
boundary cell
mypt1
single cell mosaic analysis
3D reconstruction
G
19 hpf
r3
r4
r5
mypt1 → con
H
19 hpf
mypt1 → con
I
19 hpf
rhombomere cells
boundary cells
mypt1
J
19 hpf
r3
r4
con → mypt1
K
19 hpf
con → mypt1
L
19 hpf
rhombomere cells
boundary cells
con
M
19 hpf
r3
r4
r5
con → con
N
19 hpf
con → con
O
19 hpf
rhombomere cells
boundary cells
con

Figure 4.

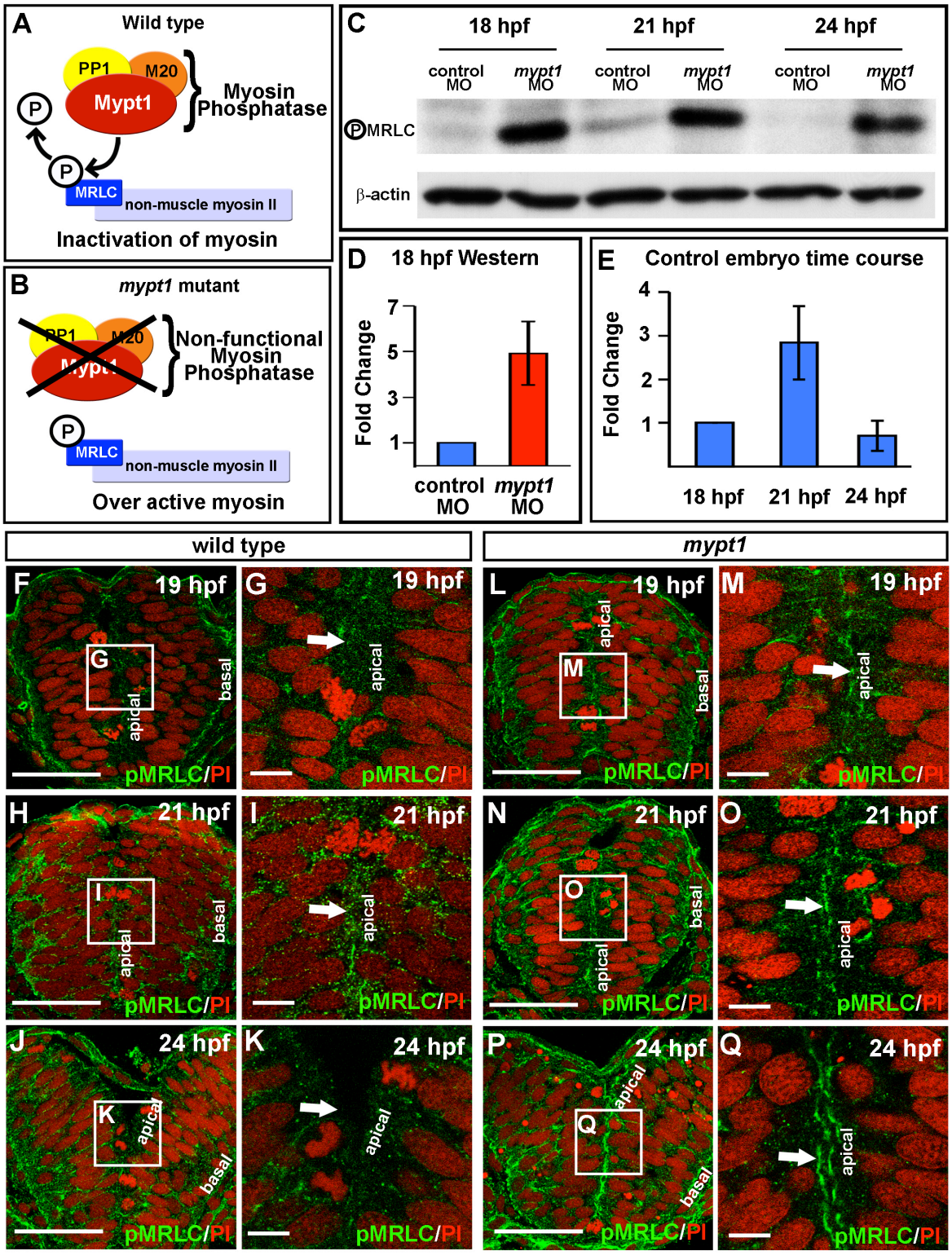
A
Wild type
PP1
M20
Mypt1
Myosin Phosphatase
P
P
MRLC
non-muscle myosin II
Inactivation of myosin
B
mypt1 mutant
Non-functional Myosin Phosphatase
P
MRLC
non-muscle myosin II
Over active myosin
C
18 hpf
21 hpf
24 hpf
control MO
mypt1 MO
PMRLC
β-actin
D
18 hpf Western
Fold Change
control MO
mypt1 MO
E
Control embryo time course
Fold Change
18 hpf
21 hpf
24 hpf
wild type
mypt1
F
G
H
I
J
K
L
M
N
O
P
Q
19 hpf
21 hpf
24 hpf
apical
basal
pMRLC/PI

Figure 5.

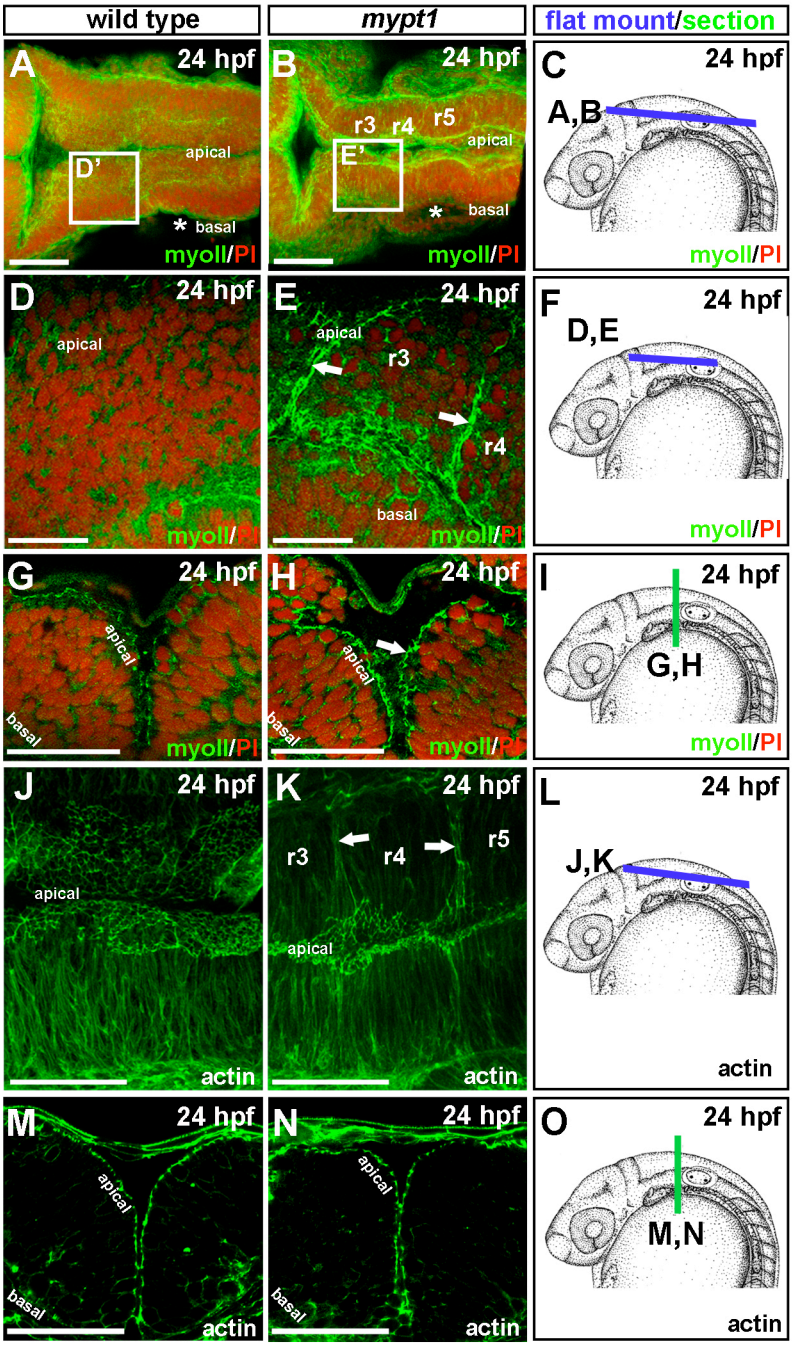
wild type
mypt1
flat mount/section
A
24 hpf
apical
D'
basal
myoII/PI
B
24 hpf
r3
r4
r5
apical
E'
basal
myoII/PI
C
24 hpf
A,B
myoII/PI
D
24 hpf
apical
myoII/PI
E
24 hpf
apical
r3
r4
basal
myoII/PI
F
24 hpf
D,E
myoII/PI
G
24 hpf
apical
basal
myoII/PI
H
24 hpf
apical
basal
myoII/PI
I
24 hpf
G,H
myoII/PI
J
24 hpf
apical
actin
K
24 hpf
r3
r4
r5
apical
actin
L
24 hpf
J,K
actin
M
24 hpf
apical
basal
actin
N
24 hpf
apical
basal
actin
O
24 hpf
M,N
actin

Figure 6.

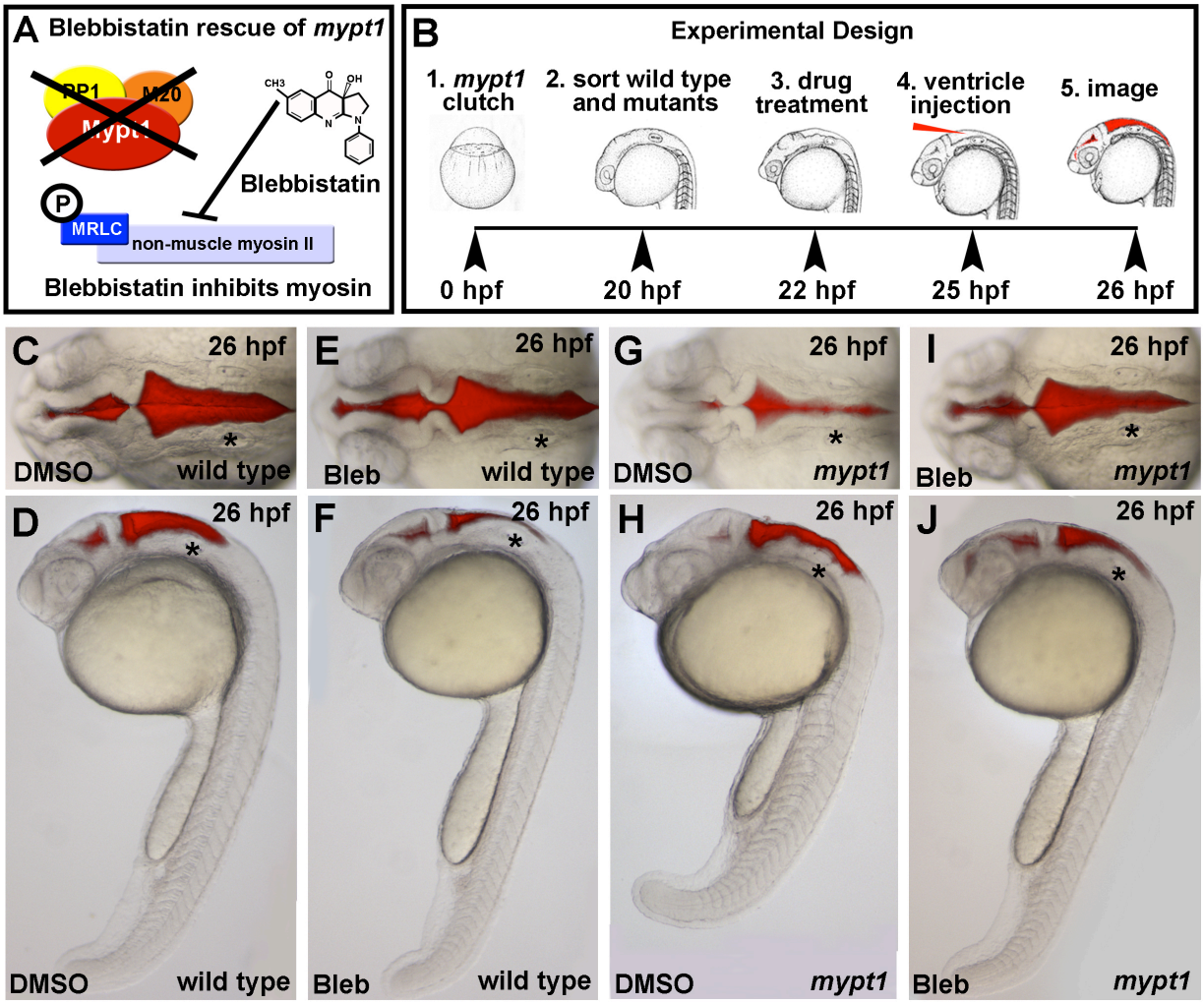
A Blebbistatin rescue of mypt1
PP1
M20
Mypt1
Blebbistatin
P
MRLC
non-muscle myosin II
Blebbistatin inhibits myosin
B
Experimental Design
1. mypt1 clutch
2. sort wild type and mutants
3. drug treatment
4. ventricle injection
5. image
0 hpf
20 hpf
22 hpf
25 hpf
26 hpf
C
26 hpf
DMSO
wild type
E
26 hpf
Bleb
wild type
G
26 hpf
DMSO
mypt1
I
26 hpf
Bleb
mypt1
D
26 hpf
DMSO
wild type
F
26 hpf
Bleb
wild type
H
26 hpf
DMSO
mypt1
J
26 hpf
Bleb
mypt1

Figure 7.

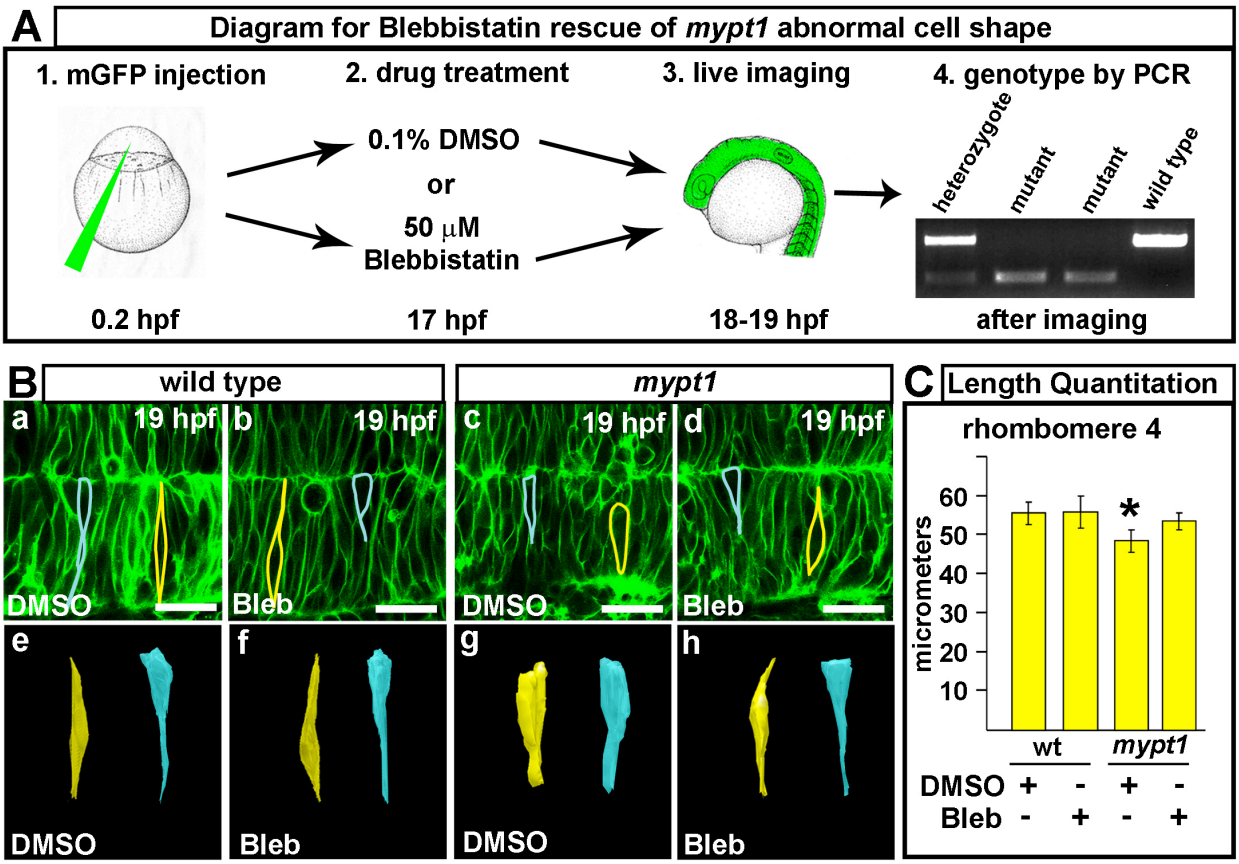
A
Diagram for Blebbistatin rescue of mypt1 abnormal cell shape
1. mGFP injection
2. drug treatment
3. live imaging
4. genotype by PCR
0.1% DMSO
or
50 μM
Blebbistatin
heterozygote
mutant
mutant
wild type
0.2 hpf
17 hpf
18-19 hpf
after imaging
B
wild type
mypt1
a 19 hpf
b 19 hpf
c 19 hpf
d 19 hpf
DMSO
Bleb
DMSO
Bleb
e
f
g
h
DMSO
Bleb
DMSO
Bleb
C
Length Quantitation
rhombomere 4
micrometers
60
50
40
30
20
10
*
wt
mypt1
DMSO + - + -
Bleb - + - +

Figure 8.

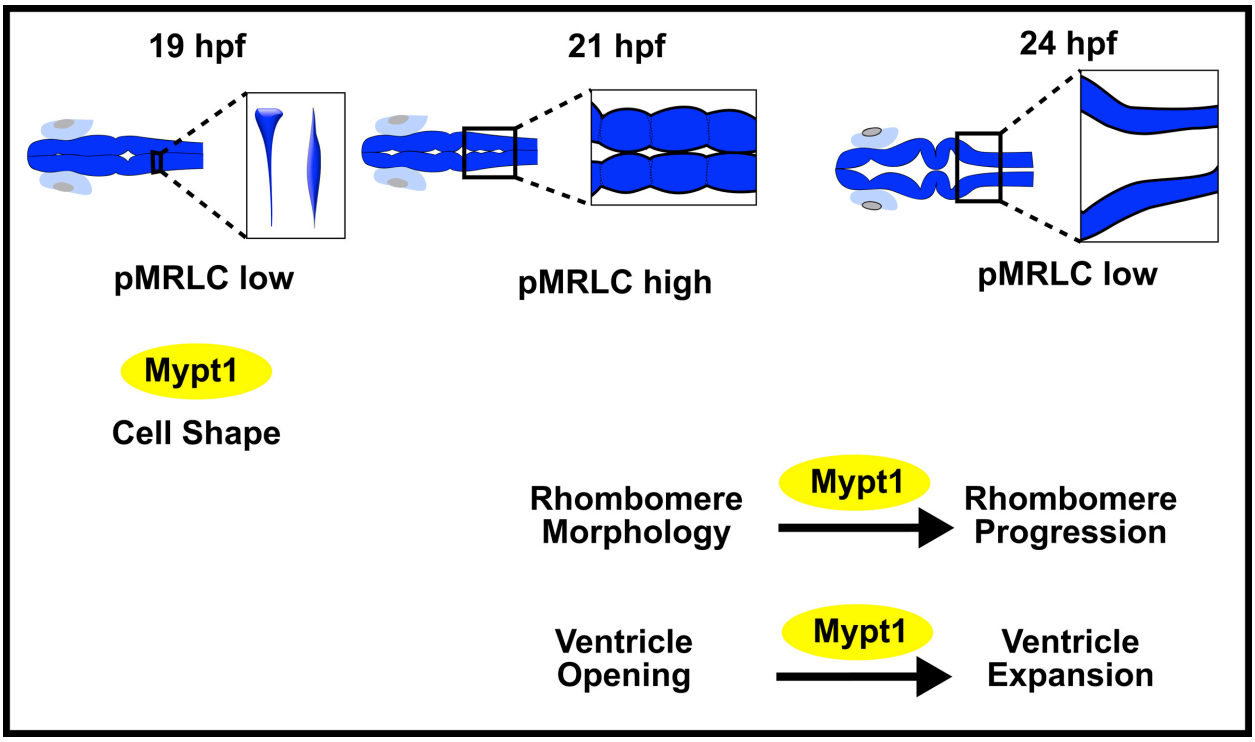
19 hpf
21 hpf
24 hpf
pMRLC low
pMRLC high
pMRLC low
Mypt1
Cell Shape
Rhombomere Morphology
Mypt1
Rhombomere Progression
Ventricle Opening
Mypt1
Ventricle Expansion